International Journal of Heat and Mass Transfer 92 (2016) 120–130

Contents lists available at ScienceDirect

International Journal of Heat and Mass Transfer

journal homepage: www.elsevier.com/locate/ijhmt

Predictions of effective thermal conductivities for three-dimensional four-directional braided composites using the lattice Boltzmann method

Wen-Zhen Fang, Li Chen, Jian-Jun Gou, Wen-Quan Tao *

Key Laboratory of Thermo-Fluid Science and Engineering, Ministry of Education, China
School of Energy & Power Engineering, Xi'an Jiaotong University, Shaanxi 710049, China

ARTICLE INFO

Article history:
Received 3 May 2015
Received in revised form 24 August 2015
Accepted 24 August 2015
Available online 9 September 2015

Keywords:
Effective thermal conductivity
Heat transfer
Braided composites
Lattice Boltzmann method

ABSTRACT

A multiple-relaxation-time lattice Boltzmann model with an off-diagonal collision matrix is adopted to predict the effective thermal conductivities of anisotropic heterogeneous materials with anisotropic components. The half lattice division scheme is used to handle the internal boundaries to guarantee the heat flux continuity at the component interfaces. Accuracy of the model is confirmed by comparing with benchmark results and existing simulation data. The present method is then employed to predict the transverse and longitudinal effective thermal conductivities of three-dimensional four-directional (3D4D) braided composites. Experiments based on the Hot Disk method are also conducted to obtain the transverse and longitudinal effective thermal conductivities of the materials. The numerically predicted results fit the experiment data well. Then, influences of fiber volume fractions, interior braiding angles and interface thermal contact resistance on the effective thermal conductivities of 3D4D braided composites are studied. The results show that the effective thermal conductivity along the transverse direction increases with the fiber volume fraction and interior braiding angle; while the longitudinal one increases with the fiber volume fraction but decreases with the increasing interior braiding angle. A larger interface thermal contact resistance leads to a smaller effective thermal conductivity. Besides, for anisotropic materials, the effective thermal conductivity obtained by the periodic boundary condition is different from that obtained by the adiabatic boundary condition.

1. Introduction

The three-dimensional four-directional (3D4D) braided composites are anisotropic heterogeneous materials composed of the matrix and braiding yarns. They have been widely applied in aeronautics and astronautics due to their high strength and low density [1]. The braiding yarns, one of the components in 3D4D braided composites, are anisotropic with different thermal conductivities along the transverse and longitudinal directions [2,3]. Heat transfer in each anisotropic component has preferable directions, and it needs a thermal conductivity matrix to fully describe the local property of components. Besides, the continuity of the normal heat flux and temperature should be ensured at the component interfaces. The thermal properties of the 3D4D braided composites are anisotropic along the transverse and longitudinal directions. For such anisotropic heterogeneous materials with anisotropic components, the effective thermal conductivity along the specified direction is an important parameter that can quantitatively evaluate the heat transfer capacity of composites. Here, several concepts are emphasized to avoid confusion. The heterogeneous material refers to a composite material with different components, and the homogenous material refers to the material with only one component. Anisotropic heterogeneous materials with anisotropic components refer to the composite materials of which the overall thermal properties are anisotropic and their components are also anisotropic. Anisotropic heterogeneous materials with isotropic components refer to the composite materials of which the overall thermal properties are anisotropic but their components are isotropic.

The lattice Boltzmann method (LBM) is an effective approach to solve the Navier–Stokes equations. It has been widely used to solve the conventional fluid flows [4,5], fluid flows in porous mediums [6,7], multiphase flows [8–10], and recently has been applied to investigate the effect of magnetic field on the behavior of the nanofluid [11,12]. Moreover, the LBM has also been used successfully in solving energy transport or mass diffusion problems. Xuan et al. [13] investigated the mass transfer process of volatile organic compounds in porous media based on the LBM. Chen et al. [14] adopted the LBM to predict the effective diffusivity of the porous gas

* Corresponding author at: Key Laboratory of Thermo-Fluid Science and Engineering, Ministry of Education, China.

http://dx.doi.org/10.1016/j.ijheatmasstransfer.2015.08.071
0017-9310/

Nomenclature

a, b, m, h	characteristic length of the unit cell, mm
c	pseudo sound speed, m/s
c_p, ρc_p	heat capacity J/(kg·K), volumetric heat capacity, J/(m^3·K)
D, d	thermal diffusivity, m^2/s, diameter of fiber, mm
$\boldsymbol{e}$	discrete velocity
f, f^{eq}	temperature distribution function, equilibrium distribution function
L	thicknesses of materials, m
$\boldsymbol{m}$	moment vector
$\mathbf{M}$	transformation matrix
q	heat flux, W/m^2
$\mathbf{S}$	relaxation time matrix
t, δt, δx	time, time step, space step
T	temperature, K
Ω	collision matrix
β, γ	oblique angle, interior braiding angle, °
ε, κ	constants, $\varepsilon = 2\ \kappa$, and $\kappa = 1/8$
ϕ	volume fraction
λ	thermal conductivity, W/(m·K)
τ	relaxation time coefficient

Subscript

α	direction of the temperature distribution function
m	matrix
f	fiber
i, j	number index
x, y, z	direction index
$\overline{\alpha}$	directions opposite to α
η, ζ	principle axis of heat conduction
e	effective
T	transverse
L	longitudinal
fy	fiber volume fraction of braiding yarn
ya	yarn volume fraction of the unit cell

diffusion layer in fuel cell. Wang et al. [15] proposed a LB algorithm to deal with the fluid–solid conjugate heat transfer problem, which can ensure the heat flux and temperature continuity at the interfaces. As for the heterogeneous materials with isotropic components, many studies have been conducted to predict their effective transport property. In particular, Wang et al. [16] proposed a LB model to predict the effective thermal conductivity for granular structures, netlike structures and fibrous structure composite materials. In the model of Wang et al. [16], the original LB Bhatnagar–Gross–Krook model was adopted, which only has a single-relaxation-time coefficient without sufficient parameters to fully describe the anisotropic heat transfer in anisotropic materials. Several studies have been conducted on the solution of anisotropic heat transfer equation using the LBM. Zhang et al. [17,18] proposed a LB model in which the relaxation time coefficients are assumed to be directionally dependent and this model ensured that the collision is mass-invariant. Ginzburg et al. [19] presented two LB models, the equilibrium-type and the link-type models, to solve the anisotropic heat transfer problems. But these models all suffer the instability and poor application flexibility [20]. Recently, the multiple-relaxation-time (MRT) LB model has been adopted for heat transfer due to its higher stability and accuracy than the single-relaxation-time model [21,22]. Yoshida and Nagaoka [20] developed a MRT LB scheme using a collision operator with off-diagonal components, making it possible to solve the anisotropic heat transfer problems, but it is only suitable for the homogeneous materials. As for the heterogeneous materials with anisotropic components, it will lead to heat flux discontinuity at the interfaces if the heat transfer at the interface is not properly treated [23].

There have been some studies using finite element methods to predict effective thermal conductivity of 3D4D braided composites [3,24,25]. However, it is quite difficult for the finite element method to consider the thermal contact resistance at the internal interface and to predict the effective thermal conductivity of heterogeneous materials with randomly distributed anisotropic components, such as needled C/SiC composites [26]. The LBM is particularly suitable for the heat and mass transfer in complex materials and has the ability to deal with the thermal contact resistance at the internal interface, and thus the present study focuses on developing a LB model for 3D4D braided composites with anisotropic components. The developed LB model can be also adopted to predict the effective thermal conductivity of the needled C/SiC composites. Besides, the previous numerical results based on the finite element method were not compared with the corresponding experimental data, and in the present study, such comparisons are also conducted.

The MRT model developed by Yoshida and Nagaoka [20] and the treatment for the internal interfaces should be combined to deal with such heterogeneous materials with anisotropic components. The single-relaxation-time LBM adopted by Wang et al. [15] is only suitable for the materials with isotropic components, and it has been used to predict the effective thermal conductivity of the isotropic heterogeneous materials with isotropic components [27] and the directional effective thermal conductivity of the anisotropic heterogeneous materials with isotropic components [28].

In the present paper, a multiple-relaxation-time LB model combined with the 'half lattice division scheme' treatment for internal interfaces is adopted to predict the effective thermal conductivity of the anisotropic heterogeneous materials with anisotropic components. The 'half lattice division scheme' first proposed by Wang et al. [15] is to handle the internal interfaces between the isotropic components. In the present paper, it is extended to deal with the internal interfaces between the anisotropic components. With the 'half lattice division scheme' method, the temperature and heat flux can be directly obtained from the local temperature distribution functions without the calculations of the finite difference, which is important for the continuity of temperature and heat flux at the interfaces (will be discussed at Section 2.3). In addition, to verify the reasonability and accuracy of the present method, several benchmarks are simulated, and then experiments based on the Hot Disk method are conducted to measure the effective thermal conductivity of 3D4D braided composites (Section 4.3). The influences of the fiber volume fraction, interior braiding yarns and interface thermal contact resistance on the effective thermal conductivity are also examined in this study (Section 5).

2. Numerical method

2.1. Governing equation

The governing equations for anisotropic heat conduction in multicomponent systems, e.g., the matrix and reinforced fibers, without any heat source can be expressed as

$$\frac{\partial T_m}{\partial t} = \frac{\partial}{\partial x_i}\left((D_{ij})_m \frac{\partial T_m}{\partial x_j} \right) \tag{1}$$

$$\frac{\partial T_f}{\partial t} = \frac{\partial}{\partial x_i}\left((D_{ij})_f \frac{\partial T_f}{\partial x_j}\right) \tag{2}$$

where the subscript m represents the matrix and f represents the reinforced fiber; T is temperature; and D_{ij} is the thermal diffusivity matrix.

At the interfaces of different components (phase), the continuity of temperature and normal heat flux should be satisfied [29]:

$$T_m = T_f \tag{3}$$

$$-n_i(\lambda_{ij})_m \frac{\partial T_m}{\partial x_j} = -n_i(\lambda_{ij})_f \frac{\partial T_f}{\partial x_j} \tag{4}$$

where n_i is the unit normal vector at the interfaces, and λ_{ij} is the thermal conductivity matrix.

2.2. MRT lattice Boltzmann model

The MRT LB model with a collision operator matrix has sufficient parameters to solve fully anisotropic heat transfer problems, and each moment can be relaxed to the equilibrium state with a different coefficient [21]. We adopt the three-dimensional seven-speed (D3Q7) model (see Fig. 1) to deal with anisotropic heat conduction problems. For the conduction process in each component of composite materials, the evolution equation of the MRT LBM for the temperature distribution functions can be expressed as [30]

$$\boldsymbol{f}(\mathbf{x} + \boldsymbol{e}_\alpha \delta t, t + \delta t) - \boldsymbol{f}(\mathbf{x}, t) = -\Omega\,(\boldsymbol{f} - \boldsymbol{f}^{\mathrm{eq}}) \tag{5}$$

where $\mathbf{x}$ denotes the particle position; t is time; δt is the time step; $\boldsymbol{f}$ is the temperature distribution function vector with seven components, denoted by $\boldsymbol{f} = (f_0, f_1, f_2, f_3, f_4, f_5, f_6)^T$; f_α^{eq} is the corresponding equilibrium temperature distribution function

$$f_\alpha^{eq} = \begin{cases} (1 - 6\kappa)T, & \alpha = 0 \\ \kappa T, & \alpha = 1, 2, \ldots, 6 \end{cases} \tag{6}$$

where $\kappa \in (0, 1/6)$. $\boldsymbol{e}_\alpha$ is the discrete velocity, defined as

$$[\boldsymbol{e}_\alpha] = [\boldsymbol{e}_0,\ \boldsymbol{e}_1,\ \boldsymbol{e}_2,\ \boldsymbol{e}_3,\ \boldsymbol{e}_4,\ \boldsymbol{e}_5,\ \boldsymbol{e}_6] = \begin{bmatrix} 0 & 1 & -1 & 0 & 0 & 0 & 0 \\ 0 & 0 & 0 & 1 & -1 & 0 & 0 \\ 0 & 0 & 0 & 0 & 0 & 1 & -1 \end{bmatrix} c \tag{7}$$

and Ω is the collision matrix

$$\Omega = \mathbf{M}^{-1}\mathbf{S}\mathbf{M} \tag{8}$$

where $\mathbf{S}$ is a relaxation time matrix, and $\mathbf{M}$ is a linear matrix that transforms the velocity space into the moment space:

$$\mathbf{M} = [\boldsymbol{\phi}_1, \boldsymbol{\phi}_2, \ldots, \boldsymbol{\phi}_7]^T, \tag{9}$$

$$\boldsymbol{m} = \mathbf{M} \cdot \boldsymbol{f} \tag{10}$$

where ϕ_α are the orthogonal basic vectors which are the polynomial functions of velocity; $\boldsymbol{m}$ is the moment vector. The definitions of the matrix $\mathbf{M}$ and the relaxation time matrix $\mathbf{S}$ are [20]:

$$\mathbf{M} = \begin{bmatrix} 1, & 1, & 1, & 1, & 1, & 1, & 1 \\ 0, & 1, & -1, & 0, & 0, & 0, & 0 \\ 0, & 0, & 0, & 1, & -1, & 0, & 0 \\ 0, & 0, & 0, & 0, & 0, & 1, & -1 \\ 6, & -1, & -1, & -1, & -1, & -1, & -1 \\ 0, & 2, & 2, & -1, & -1, & -1, & -1 \\ 0, & 0, & 0, & 1, & 1, & -1, & -1 \end{bmatrix} c \tag{11}$$

$$\mathbf{S}^{-1} = \begin{bmatrix} \tau_0, & 0, & 0, & 0, & 0, & 0, & 0 \\ 0, & \tau_{xx}, & \tau_{xy}, & \tau_{xz}, & 0, & 0, & 0 \\ 0, & \tau_{yx}, & \tau_{yy}, & \tau_{yz}, & 0, & 0, & 0 \\ 0, & \tau_{zx}, & \tau_{zy}, & \tau_{zz}, & 0, & 0, & 0 \\ 0, & 0, & 0, & 0, & \tau_4, & 0, & 0 \\ 0, & 0, & 0, & 0, & 0, & \tau_5, & 0 \\ 0, & 0, & 0, & 0, & 0, & 0, & \tau_6 \end{bmatrix} \tag{12}$$

For isotropic heat conduction problem, $\tau_{xx} = \tau_{yy} = \tau_{zz}$, and $\tau_{ij} = 0$ $(i \neq j)$. The off-diagonal components of the relaxation time matrix can take into account of the fully anisotropic heat conduction situation. For each component in composite materials, the relations between the relaxation time coefficients and the thermal diffusivity matrix of the anisotropic component can be expressed as [20,31]:

$$\begin{aligned} (\tau_{ij})_m &= \frac{1}{2}\delta_{ij} + \frac{(D_{ij})_m}{\varepsilon c^2 \delta t}, \quad i,j = 1,3 \\ (\tau_{ij})_f &= \frac{1}{2}\delta_{ij} + \frac{(D_{ij})_f}{\varepsilon c^2 \delta t}, \quad i,j = 1,3 \end{aligned} \tag{13}$$

where δ_{ij} is the Kronecker symbol, and c is the pseudo sound speed. The value of c should ensure the value of τ_{ii} $(i = 1,2,3)$ between 0.5 and 2 [26]. The values of τ_0, τ_4, τ_5, τ_6 are generally set to be unity without affecting the numerical results. If the equivalent distribution functions are defined as Eq. (6), ε equals 2κ. In this paper, the value of κ is set to be 1/8 [20].

To recover the evolution equation of discrete distribution functions to macroscopic Navier–Stokes equations, the fourth-order tensor of discrete velocities, $\sum e_{\alpha i} e_{\alpha j} e_{\alpha k} e_{\alpha l}$, should be isotropic. This

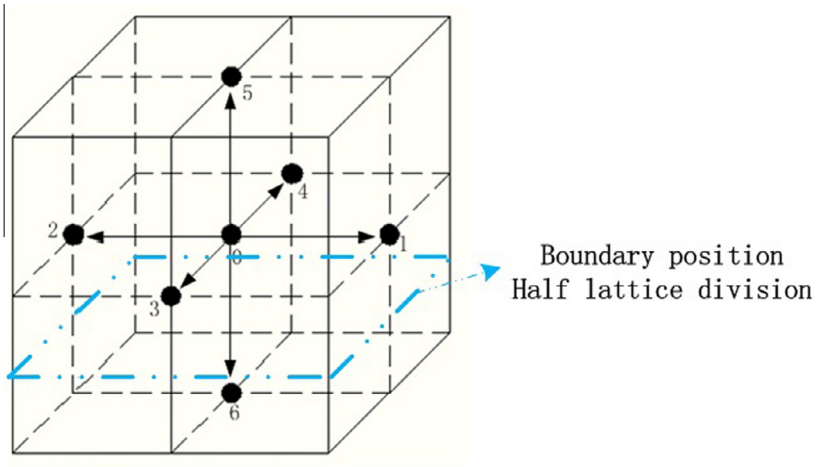

Fig. 1. D3Q7 model scheme.

isotropic requirement is not necessary for the heat diffusion equation, making it possible to minimize the numbers of discrete velocities. Therefore, we adopt the D3Q7 model instead of D3Q15 or D3Q19 model to reduce the calculation time without affecting the accuracy much. The scheme stated above has second-order accuracy with respect to the lattice interval δx and first order accuracy with respect to the time step δt [20].

2.3. Internal interfaces and boundary condition treatment

At the internal interfaces between two different components in composites, Eqs. (3) and (4) must be satisfied to ensure the continuity of temperature and heat flux. In the LBM, such conditions can be satisfied if the 'half lattice division scheme' is adopted (see Fig. 1) [15,29]. In the 'half lattice division scheme', the interface is placed at the middle of two lattice nodes. Thus, once we identify the local component to be A or B, the local temperature and heat flux can be obtained from the local temperature distribution functions without any nearby nodes information.

The local temperature can be obtained by the summation of the discrete temperature distribution functions [26]:

$$T = \sum_{\alpha} f_{\alpha} \tag{14}$$

Yoshida and Nagaoka [20] proposed the following relations between the local discrete distribution functions and the first order partial derivatives with respect to temperature

$$\begin{aligned} -\frac{1}{\varepsilon\delta x}(f_1 - f_2) &= \tau_{xx}\frac{\partial T}{\partial x} + \tau_{xy}\frac{\partial T}{\partial y} + \tau_{xz}\frac{\partial T}{\partial z} \\ -\frac{1}{\varepsilon\delta x}(f_3 - f_4) &= \tau_{yx}\frac{\partial T}{\partial x} + \tau_{yy}\frac{\partial T}{\partial y} + \tau_{yz}\frac{\partial T}{\partial z} \\ -\frac{1}{\varepsilon\delta x}(f_5 - f_6) &= \tau_{zx}\frac{\partial T}{\partial x} + \tau_{zy}\frac{\partial T}{\partial y} + \tau_{zz}\frac{\partial T}{\partial z} \end{aligned} \tag{15}$$

The first order partial derivatives with respect to temperature, $\partial T/\partial x$, $\partial T/\partial y$, $\partial T/\partial z$ can be obtained by solving the above ternary linear equations. Then, the heat fluxes along the specified directions can be calculated by

$$\begin{aligned} q_x &= \rho c_p\left(D_{xx}\frac{\partial T}{\partial x} + D_{xy}\frac{\partial T}{\partial y} + D_{xz}\frac{\partial T}{\partial z}\right) \\ q_y &= \rho c_p\left(D_{yx}\frac{\partial T}{\partial x} + D_{yy}\frac{\partial T}{\partial y} + D_{yz}\frac{\partial T}{\partial z}\right) \\ q_z &= \rho c_p\left(D_{zx}\frac{\partial T}{\partial x} + D_{zy}\frac{\partial T}{\partial y} + D_{zz}\frac{\partial T}{\partial z}\right) \end{aligned} \tag{16}$$

where ρc_p is the volumetric heat capacity.

In the conventional conjugate heat transfer problem, the general governing equation adopted for discretization in its vector form is as follows [32,33]:

$$\frac{\partial(\rho T)}{\partial t} + div(\rho \vec{U} T) = div(\Gamma grad T) + S \tag{17}$$

where Γ is the related nominal diffusion coefficient, which is defined by the following equation:

$$\Gamma = \frac{\lambda}{c_p} \tag{18}$$

Then as first pointed out by Chen and Han in [34] and later further demonstrated in [32], for a conjugate heat transfer problem if the nominal interface diffusion coefficient is determined by the harmonic mean value, the specific heat capacity (c_p) in the solid region should take the value of that in the fluid region in order to guarantee the continuity of flux at the interface.

The LB model adopted in this paper will recover to the macroscopic energy equation in the following form:

$$\frac{\partial T}{\partial t} + div(\vec{U} T) = div(D grad T) + S \tag{19}$$

Therefore, according to above discussions, we should assume:

$$(\rho c_p)_m = (\rho c_p)_f \tag{20}$$

for different phases in composites to ensure the heat flux continuity [35]. When heat transfer reaches the steady state, such treatment does not influence the temperature field. Based on this assumption (shown in Eq. (20)), the incoming distribution functions at the interfaces can be obtained by the streaming process without any additional treatment if we follow the 'half lattice division scheme':

$$\begin{aligned} f_{\overline{\alpha}}(\mathbf{x}_f, t+\delta t) &= \hat{f}_{\overline{\alpha}}(\mathbf{x}_m, t) \\ f_{\alpha}(\mathbf{x}_m, t+\delta t) &= \hat{f}_{\alpha}(\mathbf{x}_f, t) \end{aligned} \tag{21}$$

where the index $\overline{\alpha}$ indicates the directions opposite to α. Note that if the heat flux continuity at the internal interfaces needs to be satisfied in a transient analysis, the incoming distribution functions at the interfaces need to be modified. Therefore, the streaming process should be also modified at the interfaces. One can refer to Refs. [25,31] for more details. In the present paper, only the steady state is studied because it is sufficient in estimating the effective thermal conductivity of the materials.

Once the temperature field is converged, the effective thermal conductivity along specified directions can be calculated by

$$\begin{aligned} \lambda_{x,e} &= \frac{\int q_x dA_x}{(\Delta T/L_x)A_x} \\ \lambda_{y,e} &= \frac{\int q_y dA_y}{(\Delta T/L_y)A_y} \\ \lambda_{z,e} &= \frac{\int q_z dA_z}{(\Delta T/L_z)A_z} \end{aligned} \tag{22}$$

where L_x, L_y, L_z are the thicknesses of materials along x, y, z directions, respectively; q_x, q_y, q_z are steady heat fluxes along the x, y, z directions, respectively; ΔT is the temperature difference between the two opposite surfaces.

Boundary conditions for the LB simulations are as follows. For the unit cube cell of materials, two opposite boundary surfaces are set to be isothermal but at different temperature (Dirichlet condition). Other surfaces are set to be adiabatic (Neumann condition) or periodic according to the actual situation. For interfaces placed at the middle of two lattice node (see Fig. 1), the following treatments for Dirichlet and Neumann conditions have the second order accuracy [20,36].

Dirichlet condition:

$$f_{\alpha}(\mathbf{x}, t+\delta t) = -\hat{f}_{\overline{\alpha}}(\mathbf{x}, t) + \varepsilon T_d \tag{23}$$

Neumann condition:

$$f_{\alpha}(\mathbf{x}, t+\delta t) = \hat{f}_{\overline{\alpha}}(\mathbf{x}, t) + (\delta t/\delta x) q_n \tag{24}$$

While the periodic condition is expressed as follows:

$$f_{\alpha}(\mathbf{x}+L, t+\delta t) = \hat{f}_{\alpha}(\mathbf{x}, t) \tag{25}$$

here, $\hat{f}$ denotes the post-collision discrete distribution function; T_d is the given temperature and q_n is the given specified flux at the boundary.

3. Validation test

In this section, several benchmarks are simulated to validate the accuracy of the method presented in Section 2.

3.1. Infinite long anisotropic slabs

For the case in which two anisotropic thin slabs are serially connected, the effective thermal conductivity of such composite material can be obtained analytically if the geometry size along the x direction is infinite long (see Fig. 2). In Fig. 2, the oblique lines represent the principle axis of heat conduction, and β is the oblique angle. The thermal conductivities along the two principle axes of heat conduction are denoted as λ_η and λ_ζ, respectively. To obtain the effective thermal conductivity of the composites, the effective thermal conductivity of single slab along y direction, λ_y, should be first determined. The thermal conductivity matrix of the anisotropic slab in $\eta-\zeta$ coordinate is diagonal, but it should be converted into x–y coordinate:

$$\begin{bmatrix} \lambda_{xx} & \lambda_{xy} \\ \lambda_{yx} & \lambda_{yy} \end{bmatrix} = \begin{bmatrix} \cos\beta & \sin\beta \\ -\sin\beta & \cos\beta \end{bmatrix} \begin{bmatrix} \lambda_\eta & 0 \\ 0 & \lambda_\zeta \end{bmatrix} \begin{bmatrix} \cos\beta & -\sin\beta \\ \sin\beta & \cos\beta \end{bmatrix} \tag{26}$$

And the heat flux can be expressed as:

$$\begin{bmatrix} q_x \\ q_y \end{bmatrix} = -\begin{bmatrix} \lambda_{xx} & \lambda_{xy} \\ \lambda_{yx} & \lambda_{yy} \end{bmatrix} \begin{bmatrix} \frac{\partial T}{\partial x} \\ \frac{\partial T}{\partial y} \end{bmatrix} \tag{27}$$

If the slab is infinite long along the x direction, $\partial T/\partial x$ equals zero and therefore the effective thermal conductivity of the single slab along y direction, λ_y, equals λ_{yy} (according to Eq. (27)). If we assume that the two slabs have the same thickness, the effective thermal conductivity of the series slabs along y direction is equal to $2\lambda_{y1}\lambda_{y2}/(\lambda_{y1}+\lambda_{y2})$ (index 1 and 2 denote two different slabs).

We keep the ratio $\lambda_\eta = 2\lambda_\zeta$ for both slabs, and set $\lambda_{\eta1} = 2$ W/(m·K) while changing the value of $\lambda_{\eta2}$ from 2 to 2000 W/(m·K), that is, the ratio of $\lambda_{\eta2}/\lambda_{\eta1}$ varying from unity to one thousand. In our simulations, the upper and lower boundaries are set to be isothermal but at different temperature. The periodic conditions are imposed on the side boundary. The size of grid space is 0.01 at a 200×200 grid, and the value of c maintains 400,000. The effective thermal conductivities predicted by the present method and the corresponding analytical results are shown in Table 1. The maximum relative deviation is 0.003% for $\beta = 75°$ and 0.005% for $\beta = 15°$, which confirms the high accuracy of the present method.

3.2. Composites reinforced with anisotropic short fibers

Reinforced fibers are commonly dispersed in the solid matrix to increase the mechanical strength [37]. In this case, we assume that the reinforced short orthotropic fiber is transversely isotropic, i.e. $\lambda_{xx} \neq \lambda_{yy} = \lambda_{zz}$, and it is longitudinally aligned in the matrix, as shown in Fig. 3.

The fiber volume fraction, ϕ_f, and the fiber aspect ratio, ζ, are defined as

$$\phi_f = \frac{\pi d^2 l}{4a^3} \tag{28}$$

$$\zeta = \frac{l}{d} \tag{29}$$

where a is the side length of the cube; d is the fiber diameter; l is the fiber length. For a given fixed fiber volume fraction, ϕ_f, there exists a minimum fiber aspect ratio, $\zeta_{\min}$, and a maximum value, $\zeta_{\max}$ [37]:

$$\zeta_{\min} = \frac{4\phi_f}{\pi}, \quad \zeta_{\max} = \sqrt{\frac{\pi}{4\phi_f}} \tag{30}$$

To study the influences of the fiber aspect ratio on the effective thermal conductivity of composites, we keep the fiber volume fraction constant while change the fiber aspect ratio. In Ref. [37], the effective thermal conductivities of such composites are numerically estimated by the finite element method. The matrix is set to be isotropic and its thermal conductivity is assigned to be unity. The anisotropy degree of fiber is defined as $\mu = \lambda_{xx}/\lambda_{yy}$. λ_L^e and λ_T^e are the longitudinal and the transverse effective thermal conductivity of the composites, respectively. Note that the step-wise approximation is adopted to deal with the curved boundaries of the fiber. For all cases, we conducted the simulation on two grid systems $80 \times 80 \times 80$ and $60 \times 60 \times 60$ to obtain the effective thermal conductivity, and the deviations of the two grid system are within

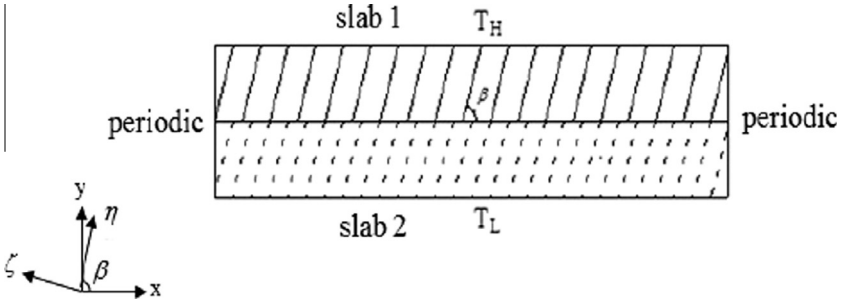

Fig. 2. Series mode of two infinite anisotropic thin slabs.

Table 1
Comparisons of the predicted results and the analytical results.

$\lambda_{\eta1}:\lambda_{\eta2}$	$\beta = 75°$			$\beta = 15°$		
	Analytical results (W/(m·K))	Predicted results (W/(m·K))	Relative deviations (%)	Analytical results (W/(m·K))	Predicted results (W/(m·K))	Relative deviations (%)
1:1	1.9330	1.9330	0	1.0670	1.0670	0
1:10	3.5145	3.5145	0	1.9400	1.9401	0.005
1:20	3.6819	3.6820	0.003	2.0324	2.0324	0
1:40	3.7717	3.7717	0	2.0820	2.0821	0.005
1:100	3.8277	3.8278	0.003	2.1129	2.1129	0
1:1000	3.8621	3.8622	0.003	2.1319	2.1320	0.005

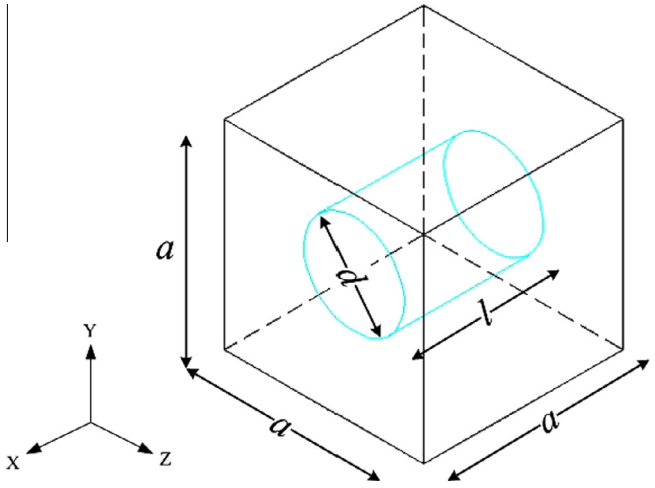

Fig. 3. Cubic-cell geometry reinforced with short fiber.

1.2%. Therefore, the grid system $60 \times 60 \times 60$ is enough for this problem. The size of grid space is 0.01 and the value of c maintains 100,000. The results based on the present method are compared with those in Ref. [37] shown in Fig. 4.

In Fig. 4(a), $\lambda_{xx} = 1000$ W/(m·K) and $\mu = 10$ for fiber; while in Fig. 4(b), $\lambda_{xx} = 100$ W/(m·K) and $\mu = 0.1$. As shown in Fig. 4, the predicted results based on the present method agree well with the existing simulation data, and the maximum deviation is 2.2%, which again confirms the accuracy of the present method.

3.3. Three-dimensional dual-component composites

A series mode of 3D dual-component composites is further considered (see Fig. 5). The thermal conductivity matrices of the two components are given as

$$\lambda_{ij}^1 = \begin{bmatrix} 4 & 1 & 2 \\ 1 & 8 & 1 \\ 2 & 1 & 10 \end{bmatrix}, \quad \lambda_{ij}^2 = \begin{bmatrix} 10 & 1 & 4 \\ 1 & 8 & 1 \\ 4 & 1 & 12 \end{bmatrix} \tag{31}$$

The boundary conditions are imposed as shown in Fig. 5. Ansys Fluent 14.0 is adopted to obtain the effective thermal conductivity of the composite material along the z direction, and it equals 10.34 W/(m·K). The result of the present LB model with a grid of $30 \times 30 \times 30$ is 10.40 W/(m·K). The deviation is 0.6%. The temperature distribution contours of the surface at the right hand side of the cube obtained by Ansys Fluent and the present method are compared in Fig. 6, which shows rather good agreement. It can be seen that at the interface, the temperature contour obtained either by Fluent or by the present method is continuous. The local normal heat flux can be obtained by Eq. (16), and it is found that the normal heat flux at the interface is also continuous with a deviation less than 0.5%. The continuity of temperature and heat flux at the interface verifies the accuracy of the present 'half lattice division scheme' treatment for the anisotropic heat conduction problem.

4. Application for 3D4D braided composites

4.1. Structure of 3D4D braided composites

For 3D4D braided composites, the inside braiding yarns are regularly woven by machines and their structure is periodic. A representative unit cell thus can be built to describe the entire composites according to the movement of braiding yarns during the braiding process, and the effective thermal conductivity of braided composites can be obtained based on such representative unit cell [2,3,38]. In the present paper, the unit cell developed in [1] is adopted, which contains 12 long straight yarns and 8 short yarns. The coordinates and orientation angles of each yarn axis are the same as those in [1,3]. A schematic of the unit cell and its components are shown in Fig. 7(a). There are two geometric scale levels: first, thousands of uniaxial fibers and the matrix constitute a braiding yarn; second, lots of braiding yarns within the matrix form the braided composites. In Fig. 7, γ is the orientation angle of each yarn with z axis, namely interior braiding angle; h denotes the braiding pitch length; and a is the side length of the unit cell. A reconstructed unit cell is shown in Fig. 7(b). In practice, the braiding yarns in composites contact tightly with each other, and each yarn is subjected to the compressive force by its adjacent yarns. As a result, the cross section of the yarns will be distorted and no longer a circle. In previous studies, different cross sections were studied, such as ellipse [2], hexagon [39] and octagon [40]. In the present work, the cross section is assumed to be ellipse. To satisfy the condition that elliptical-section braiding yarns contact tightly with each other, the sizes of the unit cell and the related geometry parameters of braiding yarns must obey the following relations [1]:

$$b = a/8 \tag{32}$$

$$m = b\sqrt{3}\cos\gamma \tag{33}$$

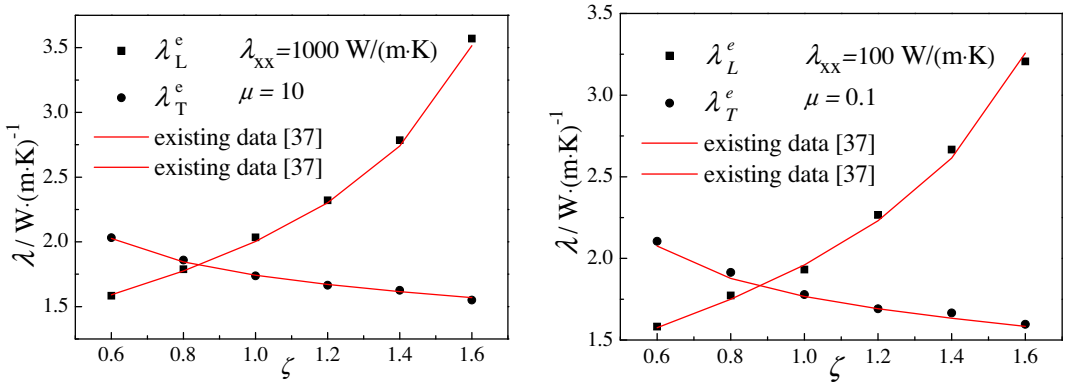

(a) λ_{xx}= 1000 W/(m·K) , μ=10 (b) λ_{xx}= 100 W/(m·K) , μ=0.1

Fig. 4. Comparisons of effective thermal conductivity between the predicted results and the existing simulation data [37].

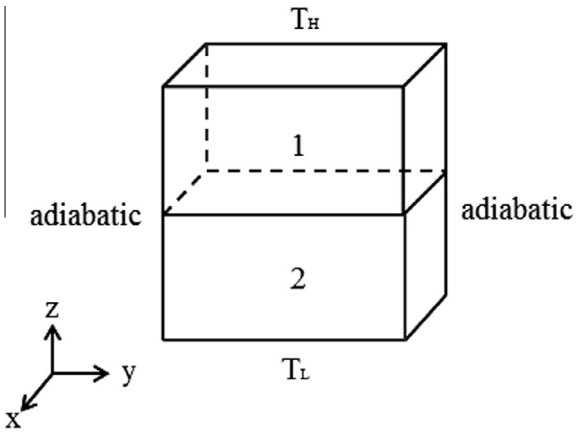

Fig. 5. Series mode of 3D dual-component composites.

$$A = \pi bm = \frac{n_f \times \pi d_f^2/4}{\phi_{fy}} \tag{34}$$

$$\phi_{ya} = \frac{(\pi mb) \times h/\cos\gamma \times 8}{a \times a \times h} = \frac{\pi\sqrt{3}}{8} = 0.68 \tag{35}$$

where m and b are the lengths of semi-major axis and semi-minor axis of the ellipse cross section, respectively; A is the area of the cross section; n_f is the number of fibers in one braiding yarn; d_f is the diameter of fibers; $\phi_{fy} = \phi_f/\phi_{ya}$ is the fiber volume fraction of the braiding yarns, ϕ_f is the fiber volume fraction of the unit cell, and ϕ_{ya} is the yarn volume fraction of the unit cell. With the given values of ϕ_f, n_f, d_f and γ, one can determine the geometry parameter values of m, b, a, h according to Eqs. (32)–(35). In the present paper, we set $n_f = 9000$, $d_f = 6.9$ μm; let γ vary from 20° to 45°, and ϕ_f equal 0.4, 0.5, 0.58.

4.2. Materials properties and boundary conditions

To determine the effective thermal conductivities of 3D4D braided composites, the thermal conductivities of their each component, matrix and braiding yarns, should be first determined. The braiding yarn, one of the components of braided composites, is composed of the matrix and thousands of uniaxial fibers. In the present paper, the matrix is epoxy resin and the reinforced fiber is T300 carbon. The thermal conductivity of isotropic resin is measured by Hot Disk TPS2500s (discussed in Section 4.3), and equals 0.178 W/(m·K). The T300 carbon fiber is transversely isotropic whose transverse and longitudinal thermal conductivities are 0.675 W/(m·K) and 7.81 W/(m·K), respectively [41]. Based on the determined thermal conductivities of the matrix resin and T300 carbon fibers, the longitudinal and transverse thermal conductivities of braiding yarns can be obtained by [25]:

$$\lambda_{ya}^L = \lambda_f^L \phi_{fy} + \lambda_m(1 - \phi_{fy}) \tag{36}$$

$$\lambda_{ya}^T = \lambda_m + \frac{(1 - \phi_{fy})}{1/\left(\lambda_f^T - \lambda_m\right) + (1 - \phi_{fy})/(2\lambda_m)} \tag{37}$$

where λ_f^L and λ_f^T are the longitudinal and transverse effective thermal conductivity of fibers, respectively; λ_m is the thermal conductivity of the matrix.

For 3D4D braided composites, two opposite surfaces along the measured direction are isothermal but at different temperature. The other boundary surfaces are imposed to be periodic [3].

4.3. Experimental measurement

In the present paper, the Hot Disk thermal constants analyzer (TPS 2500s) [42–44] based on the transient plane source method was adopted to measure the effective thermal conductivities of materials, including the isotropic resin and the anisotropic braided composites. For 3D4D braided composites, the specimens should be properly cut so that the probe can be placed perpendicular to the braiding direction.

The measurement process is as follows. The probe is clamped between two identical specimen halves, and then a heat pulse is supplied to the probe to generate a dynamic temperature field. The temperature increase of the probe surface is recorded as a function of time. The temperature response within the specimen is predominantly related to the thermal diffusivity and thermal conductivity of the measured material. By dealing with the recorded temperature curve, both the thermal conductivity and thermal diffusivity of the measured material can be obtained. For isotropic materials, the temperature increase of the probe surface can be expressed as [42]:

$$\Delta T_s(\Theta) = \frac{P_0}{\pi^{3/2} r \lambda} \mathrm{H}(\Theta) \tag{38}$$

where P_0 is the input power; r is the radius of the probe; λ is the thermal conductivity of the specimen material; $H(\Theta)$ is the dimensionless specific time function; Θ is the dimensionless time, defined as $\Theta = \sqrt{Dt}/r$, in which D is the thermal diffusivity of the specimen,

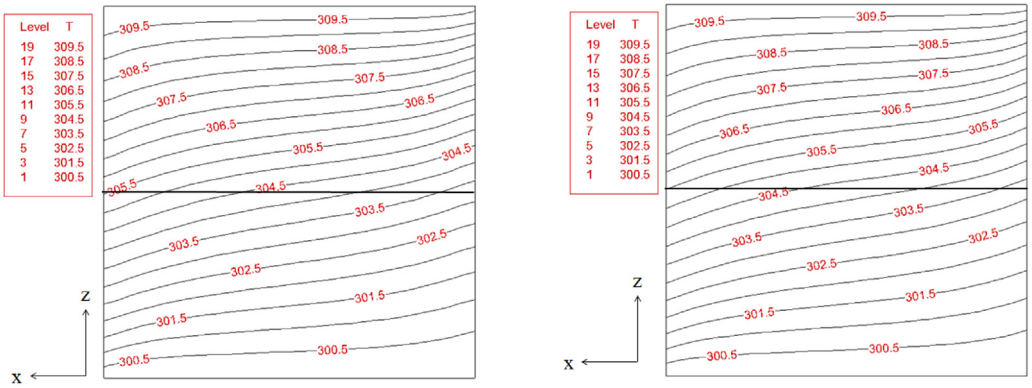

(a) By Fluent 14.0 (b) By the present method

Fig. 6. Temperature distribution contours of the right hand side surface of the cube.

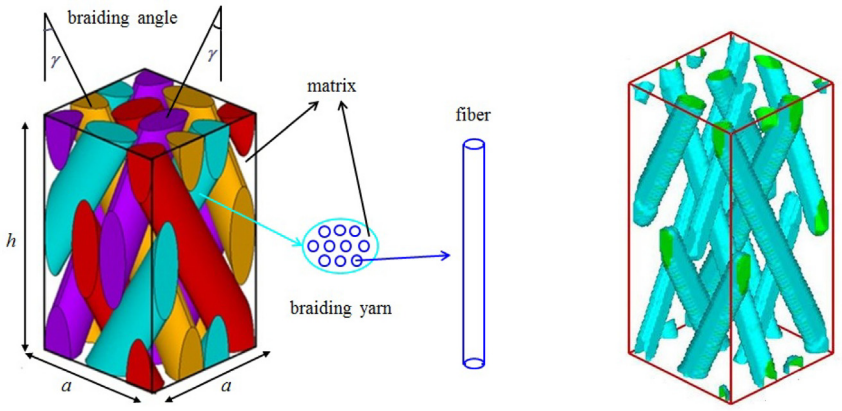

(a) The unit cell and its components (b) The reconstructed unit cell

Fig. 7. Diagram of the unit cell for 3D4D braided composites.

and t is the measurement time. The thermal diffusivity can be obtained by a least-squares procedure to obtain a best linear relation between the ΔT_s and $H(\Theta)$. Finally, the thermal conductivity can be obtained from the slope of this line (Eq. (38)).

As for anisotropic materials, the temperature increase of the probe can be expressed as [42]

$$\Delta T_s(\Theta_T) = \frac{P_0}{\pi^{3/2} r (\lambda_L \lambda_T)^{-1}} H(\Theta_T) \tag{39}$$

where λ_L and λ_T are the longitudinal and transverse effective thermal conductivities of the specimen, respectively. Similar to the isotropic case, we first obtain the thermal diffusivity of the specimen, D_T, along the transverse direction. With a given volumetric heat capacity ρc_p, we have

$$\lambda_T = \rho c_p D_T \tag{40}$$

The longitudinal thermal conductivity of the specimen, λ_L, can then be obtained from the slope of the line corresponding to Eq. (39).

5. Results and discussion

The MRT LBM combined with the 'half lattice division scheme' method presented in Section 2 is adopted to determine the longitudinal and transverse effective thermal conductivity of 3D4D braided composites. Taking the case of fiber volume fraction being 0.4 and the interior braiding angle being 25° as an example, the geometry parameters of reconstructed unit cell are as follows. The side length of the unit cell, a, is 2.724 mm; the braiding pitch length, h, is 5.843 mm; the semi-major axis of ellipse, m, is 0.535 mm; the semi-minor axis of ellipse, b, is 0.341 mm. The grid number of the reconstructed unit cell is $56 \times 56 \times 120$. The longitudinal and transverse thermal conductivities of the braiding yarns obtained from Eqs. (36) and (37) are listed in Table 2.

After reconstructing the unit cell of the composites structure and determining the thermal conductivity of each component, we can then apply the MRT LBM to calculate the effective thermal conductivities of anisotropic heterogeneous materials along the specified direction. The heat flux remains almost constant along the z direction (shown in Fig. 8), verifying the energy conservation of this method.

Table 2
Effective thermal conductivities of braiding yarns.

ϕ_f (%)	λ_{ya}^L (W/(m·K))	λ_{ya}^T (W/(m·K))
0.4	4.667	0.363
0.5	5.790	0.445
0.58	6.688	0.530

5.1. Comparisons with the experimental data

The Hot Disk thermal constants analyzer is adopted to measure the effective thermal conductivity. The experimental data and the numerical results are shown in Table 3. All the simulations are based on the assumption that the interface thermal contact resistance is negligible because different components in the composites are tightly contacted.

In Table 3, λ_T^e and λ_L^e are the numerically predicted effective thermal conductivities of 3D4D braided composites along the transverse and longitudinal directions, respectively, and λ_T and λ_L are the experimental data. The predicted results and the experimental data show good agreements and the deviations are within ±10%, confirming the accuracy of this method. In 3D4D braided composites, the braiding yarns are regularly woven by machines and their structure is periodic, making it possible to be well reconstructed. The reconstructed structure can be very similar to the real structure of composites if the fiber volume fraction and interior

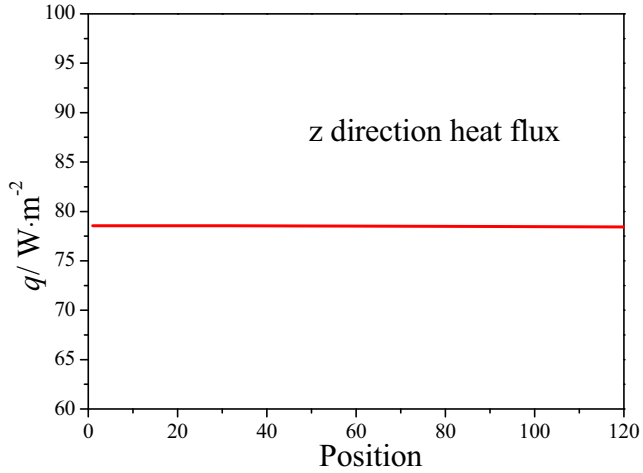

Fig. 8. Heat flux along the z direction.

Table 3
Comparisons of the experimental data and numerical results.

γ	ϕ_f	λ_T^e (W/(m·K))	λ_T (Exp) (W/(m·K))	Deviation (%)	λ_L^e (W/(m·K))	λ_L (Exp) (W/(m·K))	Deviation (%)
25	0.5	0.639	0.709	−9.87	3.085	3.41	−9.53
25	0.58	0.727	0.75	−3.07	3.444	3.52	−2.16
40	0.5	1.015	1.02	−0.4	2.258	2.50	−9.68
40	0.58	1.160	1.056	9.89	2.583	2.63	−1.78

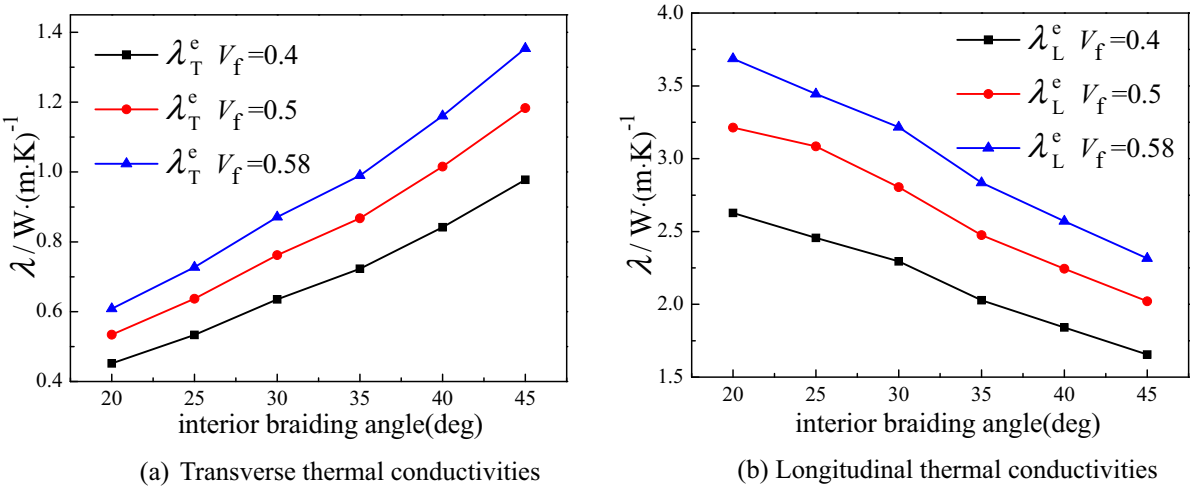

(a) Transverse thermal conductivities (b) Longitudinal thermal conductivities

Fig. 9. Effective thermal conductivities versus the interior braiding angle.

braiding angle are the same. This is exactly the reason that good agreement is obtained between the numerical results based on a representative unit cell and the experimental results based on the entire domain.

5.2. Influence of structure parameter

The influences of fiber volume fractions and interior braiding angles on the effective thermal conductivities are investigated with the fiber volume fractions as 0.4, 0.5, 0.58, and the braiding angles varying from 20° to 45°. The predicted transverse and longitudinal thermal conductivities of the 3D4D braided composites are shown in Fig. 9 (a) and (b), respectively.

It can be seen that the transverse thermal conductivity increases with the interior braiding angle, while the longitudinal thermal conductivity decreases with the increasing interior braiding angle. This can be explained as follows. A larger interior braiding angle leads to a larger proportion of yarns projected into the transverse direction, and a smaller proportion along the longitudinal direction. This indicates that the heat transfer capability is strengthened along the transverse direction but reduced along the longitudinal direction due to the bigger effective thermal conductivity of braiding yarns than that of the matrix. It can also be found that both the transverse and longitudinal effective thermal conductivity increase with the fiber volume fractions within the range of the studied interior braiding angle. This is because the thermal conductivity of fibers is bigger than that of the matrix.

It is worth mentioning that the above results are obtained based on the periodic boundary condition rather than the adiabatic one. For isotropic homogeneous or heterogeneous materials, the imposed boundary condition being either adiabatic or periodic will not influence the calculations of effective thermal conductivity. However, as for anisotropic homogeneous or heterogeneous materials, the imposed boundary condition will greatly influence the effective thermal conductivity. Taking the case of $\gamma = 25°$, $V_f = 0.5$ as an example, the transverse and longitudinal thermal conductivities are 0.637 W/(m·K) and 3.085 W/(m·K), respectively, for periodic boundary conditions, while 0.566 W/(m·K) and 2.486 W/(m·K), respectively, for adiabatic boundary conditions. The deviations between the two boundary conditions are as high as 11.1% and 19.5%, respectively. The temperature distribution contours under two different boundary conditions are shown in Fig. 10. The periodic boundary condition results in a less tortuous temperature distribution contour. This is because the periodicity means that the geometry size of measured materials along the imposed direction is infinite, and therefore the influence of the boundary on the temperature field will be reduced. For the anisotropic homogeneous materials, the periodic boundary condition results in a zero temperature gradient along the imposed direction while the adiabatic boundary condition does not. As for the anisotropic heterogeneous materials, such as the 3D4D braided composites, the temperature distribution contour obtained by periodic boundary conditions is much less tortuous than that of the adiabatic one. According to Eq. (16), the temperature gradients at x or y direction will have an influence on the heat flux along the z direction and therefore result in different effective thermal conductivities along z direction. Thus, for the simulation of the 3D4D braided composites, the periodic boundary conditions should be adopted rather than adiabatic boundary conditions.

5.3. Influence of the interface thermal contact resistance

To consider the internal thermal resistance without any model, the morphology of the contacting surface needs to be specifically described at the micro size level. It requires huge computational resources to describe such microscale morphology for the domain size studied at the millimeter level. It is still challenging to numerically consider the thermal contact resistance in the composite material. In the present paper, we embed the thermal contact resistance into the microstructure of the 3D4D braided composites.

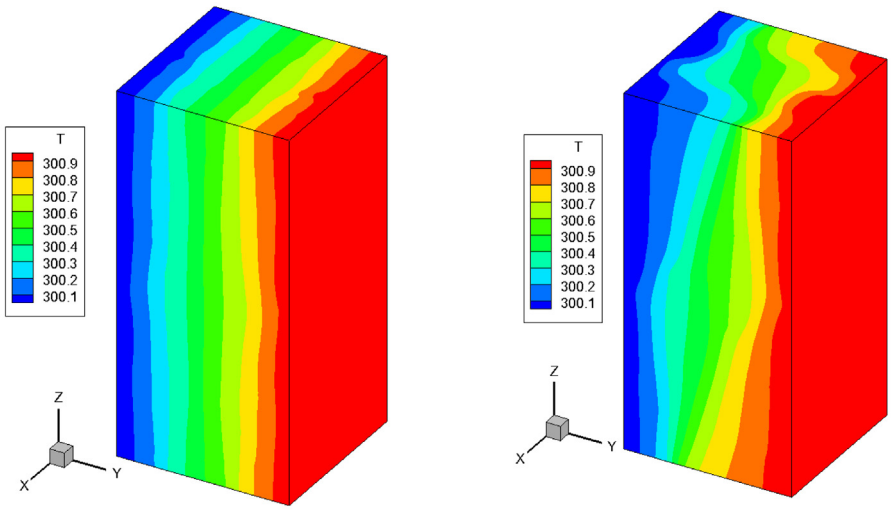

(a)The periodic boundary condition (b) The adiabatic boundary conditon

Fig. 10. Temperature distribution contours.

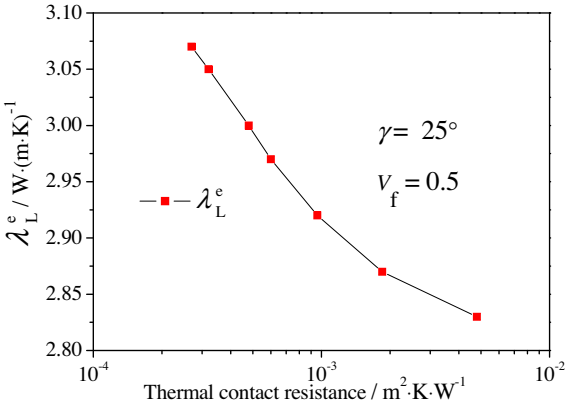

Fig. 11. The influence of the thermal contact resistance on the effective thermal conductivity.

Wang et al. [45] also adopted such method to consider the thermal contact resistance in the aerogels. At the positions of component interfaces, we use one lattice node with its local thermal conductivity less than the matrix to consider the thermal contact resistance. The local thermal conductivity of the contact nodes varies from 0.01 W/(m·K) to 0.178 W/(m·K). For the case of $\gamma = 25°$, $V_f = 0.5$, one lattice length corresponds to 48 μm length in physical unit, and therefore the corresponding thermal contact resistance varies from 0.00027 m^2·K/W to 0.0048 m^2·K/W. The influence of the thermal contact resistance on the longitudinal effective thermal conductivity of the 3D4D braided composites is shown in Fig. 11. It can be seen that the effective thermal conductivity of the 3D4D braided composites decreases when the thermal contact resistance increases.

6. Conclusions

In this paper, a multi-relaxation-time LB model combined with the 'half lattice division scheme' method is adopted to predict the effective thermal conductivities of the anisotropic heterogeneous materials with anisotropic components are also anisotropic. By benchmark validations and comparisons with the existing simulation data, the accuracy of the present method is confirmed. This method is then applied to predict the transverse and longitudinal effective thermal conductivity of 3D4D braided composites. Several corresponding experiments are conducted to measure the effective thermal conductivity of 3D4D braided composites. The LB predicted results agree well with the experimental data, verifying the accuracy of the present model. For 3D4D braided composites, it is found that both the longitudinal and transverse thermal conductivity increase with the fiber volume fraction; the transverse thermal conductivity of the braided composites increases with the interior braiding angle while the longitudinal thermal conductivity decreases when the interior braiding angle increases. A larger interface thermal contact resistance leads to a smaller effective thermal conductivity. For the simulation of the 3D4D braided composites, we should impose periodic boundary conditions rather than adiabatic boundary conditions.

It is interesting to note that the developed method can also be used to predict the effective thermal conductivity of the needled C/SiC composites, which is another type of composite materials. The results will be reported elsewhere.

Acknowledgment

This study is supported by the Key Project of International Joint Research of National Natural Science Foundation of China (51320105004).

References

[1] L. Chen, X. Tao, C. Choy, On the microstructure of three-dimensional braided preforms, Compos. Sci. Technol. 3 (59) (1999) 391–404.
[2] M.M. Shokrieh, M.S. Mazloomi, A new analytical model for calculation of stiffness of three-dimensional four-directional braided composites, Compos. Struct. 3 (94) (2012) 1005–1015.
[3] J.J. Gou, H. Zhang, Y.J. Dai, S.G. Li, W.Q. Tao, Numerical prediction of effective thermal conductivities of 3D four-directional braided composites, Compos. Struct. 125 (2015) 499–508.
[4] X. He, L.S. Luo, Theory of the lattice Boltzmann method: from the Boltzmann equation to the lattice Boltzmann equation, Phys. Rev. E 6 (56) (1997) 6811.
[5] S. Chen, G.D. Doolen, Lattice Boltzmann method for fluid flows, Annu. Rev. Fluid Mech. 1 (30) (1998) 329–364.
[6] L. Chen, G. Wu, E.F. Holby, et al., Lattice Boltzmann pore-scale investigation of coupled physical-electrochemical processes in C/Pt and non-precious metal cathode catalyst layers in proton exchange membrane fuel cells, Electrochim. Acta 158 (2015) 175–186.
[7] L. Chen, L. Zhang, Q.J. Kang, et al., Nanoscale simulation of shale transport properties using the lattice Boltzmann method: permeability and diffusivity, Sci. Rep. 5 (2014).

[8] X. He, S. Chen, R. Zhang, A lattice Boltzmann scheme for incompressible multiphase flow and its application in simulation of Rayleigh–Taylor instability, J. Comput. Phys. 2 (152) (1999) 642–663.
[9] X. Shan, H. Chen, Lattice Boltzmann model for simulating flows with multiple phases and components, Phys. Rev. E 3 (47) (1993) 1815.
[10] L. Chen, Q. Kang, Y. Mu, et al., A critical review of the pseudopotential multiphase lattice Boltzmann model: methods and applications, Int. J. Heat Mass Transfer 76 (2014) 210–236.
[11] M. Sheikholeslami, R. Ellahi, Three dimensional mesoscopic simulation of magnetic field effect on natural convection of nanofluid, Int. J. Heat Mass Transfer 89 (2015) 799–808.
[12] M. Sheikholeslami, M. Gorji-Bandpy, K. Vajravelu, Lattice Boltzmann simulation of magneto -hydrodynamic natural convection heat transfer of Al_2O_3–water nanofluid in a horizontal cylindrical enclosure with an inner triangular cylinder, Int. J. Heat Mass Transfer 80 (2015) 16–25.
[13] Y. Xuan, K. Zhao, Q. Li, Investigation on mass diffusion process in porous media based on Lattice Boltzmann method, Heat Mass Transfer 10 (46) (2010) 1039–1051.
[14] L. Chen, H.B. Luan, Y.L. He, W.Q. Tao, Pore-scale flow and mass transport in gas diffusion layer of proton exchange membrane fuel cell with interdigitated flow fields, Int. J. Therm. Sci. 51 (2012) 132–144.
[15] J. Wang, M. Wang, Z. Li, A lattice Boltzmann algorithm for fluid–solid conjugate heat transfer, Int. J. Therm. Sci. 3 (46) (2007) 228.
[16] M. Wang, N. Pan, Predictions of effective physical properties of complex multiphase materials, Mater. Sci. Eng. R 1 (63) (2008) 1–30.
[17] X. Zhang, A.G. Bengough, J.W. Crawford, I.M. Young, A lattice BGK model for advection and anisotropic dispersion equation, Adv. Water Resour. 1 (25) (2002) 1–8.
[18] X. Zhang, A.G. Bengough, L.K. Deeks, J.W. Crawford, I.M. Young, A novel three-dimensional lattice Boltzmann model for solute transport in variably saturated porous media, Water Resour. Res. 9 (38) (2002) 6-1–6-10.
[19] I. Ginzburg, Equilibrium-type and link-type lattice Boltzmann models for generic advection and anisotropic-dispersion equation, Adv. Water Resour. 11 (28) (2005) 1171–1195.
[20] H. Yoshida, M. Nagaoka, Multiple-relaxation-time lattice Boltzmann model for the convection and anisotropic diffusion equation, J. Comput. Phys. 20 (229) (2010) 7774–7795.
[21] I. Rasin, S. Succi, W. Miller, A multi-relaxation lattice kinetic method for passive scalar diffusion, J. Comput. Phys. 2 (206) (2005) 453–462.
[22] D. Humières, Multiple–relaxation–time lattice Boltzmann models in three dimensions, Philos. Trans. R. Soc. London Ser. A 1792 (360) (2002) 437–451.
[23] H. Karani, C. Huber, Lattice Boltzmann formulation for conjugate heat transfer in heterogeneous media, Phys. Rev. E 2 (91) (2015) 023304.
[24] Z. Lu, C. Wang, B. Xia, Y. Zhou, Effect of interfacial properties on the thermophysical properties of 3D braided composites: 3D multiscale finite element study, Polym. Compos. 9 (35) (2013) 1690–1700.
[25] Z. Liu, H. Zhang, Z. Lu, D. Li, Investigation on the thermal conductivity of 3-dimensional and 4-directional braided composites, Chin. J. Aeronaut. 4 (20) (2007) 327–331.
[26] Y. Cai, Y.D. Xu, B. Li, et al., Microstructures and mechanical properties of a low-cost three-dimensional needled carbon/silicon carbide composite, Mater. Sci. Eng. A 1 (497) (2008) 278–282.
[27] M. Wang, J. Wang, N. Pan, S. Chen, Mesoscopic predictions of the effective thermal conductivity for microscale random porous media, Phys. Rev. E 3 (75) (2007) 036702.
[28] E. Chiavazzo, P. Asinari, Reconstruction and modeling of 3D percolation networks of carbon fillers in a polymer matrix, Int. J. Therm. Sci. 12 (49) (2010) 2272–2281.
[29] L. Li, C. Chen, R. Mei, J.F. Klausner, Conjugate heat and mass transfer in the lattice Boltzmann equation method, Phys. Rev. E 4 (89) (2014) 043308.
[30] A. Mohamad, Lattice Boltzmann Method, Springer, 2011.
[31] H. Yoshida, T. Kobayashi, H. Hayashi, T. Kinjo, H. Washizu, K. Fukuzawa, Boundary condition at a two-phase interface in the lattice Boltzmann method for the convection-diffusion equation, Phys. Rev. E 1 (90) (2014) 013303.
[32] W.Q. Tao, Numerical Heat Transfer, Xi'an Jiaotong University Press, Xi'an, 2001. pp. 483–487.
[33] S. Patankar, Numerical Heat Transfer and Fluid Flow, CRC Press, 1980.
[34] X. Chen, P. Han, A note on the solution of conjugate heat transfer problems using simple-like algorithms, Int. J. Heat Fluid Flow 4 (21) (2000) 463–467.
[35] M. Wang, J. He, J. Yu, N. Pan, Lattice Boltzmann modeling of the effective thermal conductivity for fibrous materials, Int. J. Therm. Sci. 9 (46) (2007) 848–855.
[36] L. Li, R. Mei, J.F. Klausner, Boundary conditions for thermal lattice Boltzmann equation method, J. Comput. Phys. 237 (2013) 366–395.
[37] C.F. Matt, M.E. Cruz, Enhancement of the thermal conductivity of composites reinforced with anisotropic short fibers, J. Enhanc. Heat Transfer 1 (13) (2006) 17–38.
[38] T. Zeng, L.Z. Wu, L.C. Guo, Mechanical analysis of 3D braided composites: a finite element model, Compos. Struct. 3 (64) (2004) 399–404.
[39] D.S. Li, Z.X. Lu, L. Chen, J.L. Li, Microstructure and mechanical properties of three-dimensional five-directional braided composites, Int. J. Solids Struct. 18 (46) (2009) 3422–3432.
[40] X. Yu, J. Cui, The prediction on mechanical properties of 4-step braided composites via two-scale method, Compos. Sci. Technol. 3 (67) (2007) 471–480.
[41] Y. Yamashita, H. Yamada, H. Miyake, Effective thermal conductivity of plain weave fabric and its composite material made from high strength fibers, J. Text. Eng. 4 (54) (2008) 111–119.
[42] ISO22007-2, Plastics-determination of thermal source (hot disc) method, 2008.
[43] H. Zhang, Y. Jin, W. Gu, Z.Y. Li, W.Q. Tao, A numerical study on the influence of insulating layer of the hot disk sensor on the thermal conductivity measuring accuracy, Prog. Comput. Fluid Dyn. 3–4 (13) (2013) 191–201.
[44] L. Ma, R. Srivastava, D. Barpanda, T. Fowler, T. Theophanous, N. Verghese, An inverse approach to characterize anisotropic thermal conductivities of a dry fibrous preform composite, J. Reinf. Plast. Compos. 32 (2013) 1916–1927.
[45] M. Wang, X. Wang, J. Wang, et al., Grain size effects on effective thermal conductivity of porous materials with internal thermal contact resistance, J. Porous Media 11 (16) (2013) 1043–1048.